Preparation and Adsorption Properties for Thiophene of Nanostructured W_2C on Ultrahigh-Surface-Area Carbon Materials

Changhai Liang,*,† Fuping Tian,†,‡ Zhonglai Li,† Zhaochi Feng,† Zhaobin Wei,† and Can Li†

State Key Laboratory of Catalysis, Dalian Institute of Chemical Physics, Chinese Academy of Sciences, 457 Zhongshan Road, Dalian 116023, China, and State Key Laboratory of Fine Chemical Engineering, Dalian University of Technology, 158 Zhongshan Road, Dalian 116012, China

Received May 23, 2003. Revised Manuscript Received October 1, 2003

Nanostructured tungsten carbides on ultrahigh-surface-area carbon (>3000 m^2/g), a kind of novel carbon material with uniform pore distribution, have been prepared by carbothermal reduction, carbothermal hydrogen reduction, and metal-promoted carbothermal hydrogen reduction under mild conditions. The resulting carbides have been characterized by X-ray diffraction, transmission electron microscopy, temperature-programmed reduction−mass spectroscopy, and N_2 physico-sorption. The adsorption properties of thiophene on nanostructured tungsten carbides on ultrahigh-surface-area carbon were also investigated in a fixed-bed reactor. The results show that nanostructured W_2C particles of about 10 nm on ultrahigh-surface-area carbon material can be synthesized by carbothermal reduction and carbothermal hydrogen reduction at 850 °C. Nanostructured W_2C has also been obtained by metal Ni-promoted carbothermal hydrogen reduction even at 650 °C. The results also show that carbothermal hydrogen reduction can form tungsten carbides under relatively mild conditions compared to carbothermal reduction, and addition of Ni further decreases formation temperatures of tungsten carbides. Tungsten carbides formation involves the sequence $WO_3 \rightarrow WO_x$ $(0 < x < 3) \rightarrow W \rightarrow W_2C \rightarrow WC$. The results on adsorption show that W_2C/HSAC has superior properties for removal of sulfur-containing compounds in fuel oil and the adsorption properties can be recovered after H_2 reduction at 800 °C. The adsorption capacity of the samples on thiophene is in the following order: W_2C/HSAC > W/HSAC > WC/HSAC ≫ HSAC. Nanostructured W_2C/HSAC may be of great potential in ultra-deep removal of sulfur-containing compounds in fuel oil.

Introduction

Transition metal carbides have received considerable attention for their unique physical and chemical properties.[1,2] They have been widely used in cutting tools, abrasives, and hard coatings, and as electronic and magnetic materials and superconductors.[2] Transition metal carbides have been studied as catalytic materials and were found to show exceptionally high activities,[3−10] similar to those of noble metal catalysts in hydrogen-involving reactions, such as ammonia synthesis and decomposition,[11] Fischer−Tropsch synthesis,[12] hydrogenation,[13,14] and hydrotreating,[15−18] and may be functionalized using alkylidene layers.[19]

Conventional preparation methods for carbides have been inherited from the metallurgical industry and involve reaction of metal compounds with graphitic carbon at high temperatures. The resulting carbides have a low specific surface area and are unsuitable for

* To whom correspondence should be addressed. Phone: 86-411-4379303. Fax: 86-411-4694447. E-mail: chliang@dicp.ac.cn. Homepage: http://www.canli.dicp.ac.cn/liangch.htm.
† State Key Laboratory of Catalysis.
‡ State Key Laboratory of Fine Chemicals Engineering.

(1) Toth, L. E. *Transition Metal Carbides and Nitrides*; Academic Press: New York, 1971.
(2) Oyama, S. T. *The Chemistry of Transition Metal Carbides and Nitrides*; Blackie Academic & Professional: Glasgow, 1996.
(3) Levy, R. B.; Boudart, M. *Science* **1973**, *181*, 547.
(4) Ribeiro, F. H.; Boudart, M.; Dalla Betta, R. A.; Iglesia, E. *J. Catal.* **1991**, *130*, 498.
(5) Ross, P. N.; Stonehart, P. *J. Catal.* **1977**, *48*, 42.
(6) Iglesia, E.; Ribeiro, F. H.; Boudart, M.; Baumgartner, J. E. *Catal. Today* **1992**, *15*, 307.
(7) Sherif, F.; Vreugenhil, W. In *The Chemistry of Transition Metal Carbides and Nitrides*; Oyama, S. T., Ed.; Blackie Academic & Professional: Glasgow, 1996; pp 414−425.
(8) Lee, J. S.; Yeom, M. H.; Park, K. Y.; Nam, I. S.; Chung, J. S.; Kim, Y. G.; Moon, S. H. *J. Catal.* **1991**, *128*, 126.
(9) Keller, V.; Weher, P.; Garin, F.; Ducros, R.; Maire, G. *J. Catal.* **1995**, *153*, 9.
(10) Leclercq, L.; Provost, M.; Leclercq, G. *J. Catal.* **1989**, *117*, 384.
(11) Oyama, S. T. *Catal. Today* **1992**, *15*, 179.
(12) Ranhotra, G. S.; Bell, A. T.; Reimer, J. A. *J. Catal.* **1987**, *108*, 40.
(13) Kojima, I.; Miyazaki, E.; Inoue, Y.; Yasumori, I. *J. Catal.* **1982**, *73*, 128.
(14) Woo, H. C.; Park, K. Y.; Kim, Y. G.; Nam, I. S.; Chung, J. S.; Lee, J. S. *Appl. Catal.* **1991**, *75*, 267.
(15) McCrea, K. R.; Logan, J. W.; Tarbuck, T. L.; Heiser, J. L.; Bussell, M. E. *J. Catal.* **1997**, *171*, 255.
(16) Oyama, S. T.; Yu, C. C.; Ramanathan, S. *J. Catal.* **1999**, *184*, 535.
(17) Yu, C. C.; Ramanathan, S.; Dhandapani, B.; Chen, J. G.; Oyama, S. T. *J. Phys. Chem. B* **1997**, *101*, 512.
(18) Schwarttz, V.; Oyama, S. T.; Chen, J. G. *J. Phys. Chem. B* **2000**, *104*, 8800.
(19) Zahidi, E. M.; Oudghiri-Hassani, H.; McBreen, P. H. *Nature* **2001**, *409*, 1023.

10.1021/cm034399c CCC: $25.00
Published on Web 11/14/2003

use as catalytic materials and adsorbents. Many methods, including gas-phase reactions of volatile metal compounds, reaction of gaseous reagents with solid-state metal compounds, pyrolysis of metal complexes and solution reactions, have been developed for the preparation of high-surface-area carbides[2,20−22] in order to optimize application of the carbides in catalysis and adsorption. It is also found that the catalytic and adsorptive properties of carbide materials strongly depend on their surface structure and composition, which are closely associated with the preparation methods. A representative method of preparing transition metal carbides with high surface area or nanoscale particles is the temperature-programmed reaction between oxide precursors and a flowing mixture of hydrogen and the carbon-containing gases, such as CH_4,[23−25] C_2H_6,[26−28] C_4H_{10},[29−31] and CO.[32] The method had been widely used to synthesize transition metal carbides for catalysis. However, the resulting carbide surface from the method is usually contaminated by polymeric carbon from the pyrolysis of the containing-carbon gases, and the carbon blocks in the pores, covers the active sites, and is difficult to remove.

Ledoux and co-workers developed a novel synthesis route to preparing high-surface-area carbides which can avoids the formation of carbon residues on the surface.[33−36] It involves the reaction of solid carbon with vaporized metal oxides at very high temperatures, even above 1000 °C. Activated carbon was used as the carbon source and the final carbides appeared to retain the characteristics of the porous structure of the activated carbon. Moene et al. described a catalytic carbothermal method for converting carbon materials to high-surface-area SiC.[37,38] Mordenti et al. modified a carbothermal method and prepared activated-carbon-supported Mo_2C samples under moderate temperature.[39] We have prepared nanostructured Mo_2C and Co_3Mo_3C using carbon material as carbon source and support by carbothermal hydrogen reduction[40−42] and found that carbothermal hydrogen reduction is a useful and simple way to synthesize nanostructured carbides under mild conditions.

Table 1. Surface Area, Porosity, and Average Pore Size of HSAC and the Samples with Different W Loadings Prepared by Carbothermal Hydrogen Reduction at 850 °C

sample	BET surface area (m^2/g)	pore volume (cm^3/g)	average pore size (Å)
HSAC	3234	1.78	22.0
W/HSAC-5%	3030	1.68	21.6
W/HSAC-10%	2536	1.45	21.8
W/HSAC-15%	2419	1.33	22.8
W/HSAC-20%	2232	1.16	23.6

Tungsten carbides can be prepared by the temperature-programmed reaction for carbides synthesis. Temperature-programmed synthesis using hydrogen/hydrocarbon mixtures results in stoichiometric WC.[6] However, high-surface-area W_2C was synthesized through a topotactic conversion of intermediate tungsten nitrides using ammonia as the nitriding agent.[23] W_2C directly from the temperature-programmed synthesis using hydrogen/hydrocarbon gives a very low surface area. Sherif and Vreugdenhil used the pyrolysis of an organometallic complex to synthesize W_2C.[7] Ledoux et al. reported that the reaction of WO_2 vapors with activated carbon under vacuum at 1273−1523 K led to W_2C and WC mixture with high surface area.[34] But the reaction conditions are severe and not facile to carry out. Therefore, in this work, for the first time, we report the synthesis of nanostructured tungsten carbides on ultrahigh-surface-area carbon material via carbothermal hydrogen reduction and metal-promoted carbothermal hydrogen reduction under relatively mild conditions. The formation mechanism was also studied by using XRD and TPR−MS. The resulting nanostructured tungsten carbides are shown to have high adsorption capacity for thiophene.

Experimental Section

Ultrahigh-surface-area carbon material[43] is made by a direct chemical activation route in which petroleum coke is reacted with excess KOH at 900 °C to produce the carbon materials containing potassium salts. These salts are removed by successive water washings. The surface area of the carbon materials measured by BET method is about 3234 m^2/g, the pore volume is about 1.78 m^3/g, and the average pore size is about 2.2 nm (Table 1). More details on the preparation of this material and extensive characterization studies are reported elsewhere.[44] The surface area of the sample was measured by BET method for several times and the results were consistently in the range of 3100−3300 m^2/g. This value underscores the extraordinary nature of ultrahigh-surface-area carbon material. The theoretical maximum for surface area based on monolayer of carbon, including the area on both sides of the

(20) Oyama, S. T. In *Handbook of Heterogeneous Catalysis*; Ertl, G., Knozinger, H., Weitkamp, J., Eds.; Wiley-VCH: Weinheim, Germany, 1997; pp 132−138 and references therein.
(21) Nelson, J. A.; Wagner, M. *J. Chem. Mater.* **2002**, *14*, 1639.
(22) Johnson, C.; Sellinschegg, H.; Johnson, D. C. *Chem. Mater.* **2001**, *13*, 3876.
(23) Volpe, L.; Bourdart, M. J. *Solid State Chem.* **1985**, *59*, 348.
(24) Lee, J. S.; Volpe, L.; Ribeiro, F. H. Bourdart, M. *J. Catal.* **1988**, *112*, 44.
(25) Lee, J. S.; Oyama, S. T.; Bourdart, M. *J. Catal.* **1987**, *106*, 125.
(26) Claridge, J. B.; York, A. P. E.; Brungs, A. J.; Green, M. L. *H. Chem. Mater.* **2000**, *12*, 132.
(27) Xiao, T. C.; York, A. P. E.; Al-Megren, H.; Williams, C. V.; Wang, H. T.; Green, M. L. H. *J. Catal.* **2001**, *202*, 100.
(28) Hanif, A.; Xiao, T. C.; York, A. P. E.; Sloan, J.; Green, M. L. H. *Chem. Mater.* **2002**, *14*, 1009.
(29) Xiao, T. C.; York, A. P. E.; Williams, C. V.; Al-Megren, H.; Hanif, A.; Zhou, X.; Green, M. L. H. *Chem. Mater.* **2000**, *12*, 3896.
(30) Xiao, T. C.; Wang, H. T.; York, A. P. E.; Williams, V. C.; Green, M. L. H. *J. Catal.* **2002**, *209*, 318.
(31) Yuan, S. D.; Derouane-Abd Hamid, S. B.; Li, Y. X.; Ying, P. L.; Xin, Q.; Rass, R.; Derouane, E. G.; Li, C. J. *Mol. Catal. A* **2002**, *184*, 257.
(32) Lemaitre, J.; Vidick, B.; Delmon, B. *J. Catal.* **1986**, *99*, 415.
(33) Ledoux, M. J.; Hantzer, J.; Guille, J.; Dubots, D. U.S. Patent 4,914,070 1990.
(34) Ledoux, M. J.; Hantzer, J.; Pham-Huu, C.; Guille, J.; Desaneaux, M. P. *J. Catal.* **1988**, *114*, 176.
(35) Meunier, F.; Deporte, P.; Heinrich, B.; Bouchy, C.; Crouzet, C.; Pham-Huu, C.; Panissod, P.; Lerou, J. J.; Mills, P. L.; Ledoux, M. J. *J. Catal.* **1997**, *169*, 33.
(36) Ledoux, M. J.; Pham-Huu, C. *CATTECH* **2001**, *5*, 226.
(37) Moene, R.; Kramer, L. F.; Schoonman, J.; Makkee, M.; Moulijn, J. A. *Appl. Catal.* **1997**, *162*, 181.
(38) Moene, R.; Makkee, M.; Moulijn, J. A. *Catal. Lett.* **1995**, *34*, 285.
(39) Mordenti, D.; Brodzki, D.; Djega-Mariadassou, G. J. *Solid State Chem.* **1998**, *141*, 114.
(40) Liang, C. H.; Ying, P. L.; Li, C. *Chem. Mater.* **2002**, *14*, 3148.
(41) Liang, C. H.; Wei, Z. B.; Xin, Q.; Li, C. *Stud. Surf. Sci. Catal.* **2002**, *143*, 975.
(42) Liang, C. H.; Ma, W. P.; Feng, Z. C.; Li, C. *Carbon* **2003**, *41*, 1833.
(43) Grunewald, G. C.; Drago, R. S. *J. Am. Chem. Soc.* **1991**, *113*, 1636.
(44) O'Grady, T. M.; Wennerberg, A. N. *High-Surface-Area Active Carbon*; ACS Symposium Series 303; American Chemical Society: Washington, DC, 1986.

plane, is 2620 m^2/g. Exposure of both sides of every carbon atom is impossibile for a solid with any physical integrity. Thus, these compounds are on the threshold of sensitivity for surface area measurement techniques and are among the most porous materials ever synthesized.

The ultrahigh-surface-area carbon material was impregnated in a rotary evaporator at room temperature with an aqueous solution of ammonium paratungstate hexahydrate or an aqueous solution of ammonium paratungstate hexahydrate and nickel nitrate mixture. For WO_3/HSAC samples, tungsten content was about 5, 10, 15, and 20 wt. %, respectively. And for the NiWOx/HSAC sample, Ni/W molar ratio was about 0.2. After evaporating and drying in air at 120 °C overnight, the samples were transferred to a quartz reactor inside a tubular resistance furnace controlled by temperature programmer. The amount of the samples was about 4 g/batch. Pure hydrogen was passed through the sample at a flow rate of 200 cm^3/min. The temperature was increased at a linear rate of 1 °C/min to the final temperature, which was held for 1 h. The samples were quenched to room temperature in flowing argon, and then passivated by 1% O_2/N_2 mixture.

X-ray diffraction analysis of the samples was carried out using a Rigaku D/Max-RB diffractometer with Cu Kα monochromatized radiation source ($\lambda = 1.54178$ Å), operated at 40 KV and 100 mA. The average size of tungsten carbide particles was evaluated by the Scherrer formula from the half-width of the XRD peak corrected for instrumental broadening.

$$L = \frac{0.9\lambda_{K\alpha_1}}{B_{(2\theta)}\cos\theta_{\max}}$$

where $\lambda_{K\alpha_1}$ is 1.54178 Å, $B_{(2\theta)}$ is a full width at half-maximum of diffraction peak in radians. The molar fraction x of W_2C in a $W_2C-WC-W$ mixture was calculated from XRD patterns as

$$x = \frac{S_1}{S_1 + S_2 + S_3}$$

where S_1, S_2, and S_3 are the peak areas of the most intense reflections of W_2C, WC, and W, respectively.

The morphology and the particle size and distribution of the samples were studied by transmission electron microscopy (TEM) in a JEOL 2000 TEM operating at 100 kV.

Temperature-programmed reduction (TPR) of the sample was carried out in a stream of 95% argon and 5% hydrogen with a flow rate of 30 cm^3/min. The catalyst bed was heated linearly at 20 °C/min from room temperature to 950 °C. A Omnistar 300 quadrupole mass spectrometer was used as detector.

Nitrogen adsorption and desorption isotherms were measured with multi-point method at 77 K using a Micromertics 2010. Prior to the measurements all samples (about 0.2 g of sample between 160 and 200 mesh) were degassed at a temperature of 300 °C at vacuum level of 10^{-3} Torr for at least 3 h. Surface areas were calculated from the linear part of the Brunauer−Emmett−Teller (BET) plot.

To estimate the adsorption properties of nanostructured tungsten carbides on ultrahigh-surface-area carbon, the dynamic adsorption experiment of thiophene was carried out using a fixed-bed reactor. Prior to adsorption, the carbide samples were reduced again in the fixed-bed reactor with hydrogen at 500 °C for 2 h to remove contaminents on the carbides. A heptane solution containing thiophene (S content 740 ng/mL) passed through the fixed-bed reactor at room temperature (about 25 °C) and ambient pressure. Operating conditions were as follows: flow rate 3 mL/h; amount of carbide samples 0.1840 g. Sulfur content of effluent was analyzed by microcoulometry every 30 min.

Results and Discussion

Synthesis of W_2C/HSAC via Carbothermal Reduction. Figure 1 shows XRD patterns of WO_3/HSAC samples with tungsten loading of 10 wt % by carbothermal reduction (CR). XRD patterns of the samples with carbothermal reduction at 600 and 700 °C give typical diffraction peaks at 13.88, 23.54, 27.82, 36.86, and 49.29°, which are due to tungsten oxides such as WO_3, WO_2, and $WO_{2.9}$. The results indicate that WO_3 is first reduced to WO_2 via $WO_{2.9}$ during carbothermal reduction. The XRD pattern of the sample by carbothermal reduction at 800 °C shows diffraction peaks of metal tungsten at 40.12, 58.29, and 73.18°, indicating tungsten oxides are further reduced to metal tungsten. At the same time, weak peaks at 34.32, 37.79, and 39.40° were also detected, which can be assigned to W_2C with hexagonal closed-packed structure (lattice parameters $a = 0.300$ nm and $c = 0.473$ nm). When the temperature increases up to 850 °C, the peaks due to W_2C become sharper, and the peaks due to metal tungsten become weaker. By further increasing temperatures of carbothermal reduction to 900 °C, two new diffraction peaks at 35.44 and 48.16° were observed besides the diffraction peaks due to W_2C. The two diffraction peaks at 35.44 and 48.16° can be attributed to WC with hexagonal closed-packed structure (lattice parameters $a = 0.291$ nm and $c = 0.284$ nm).

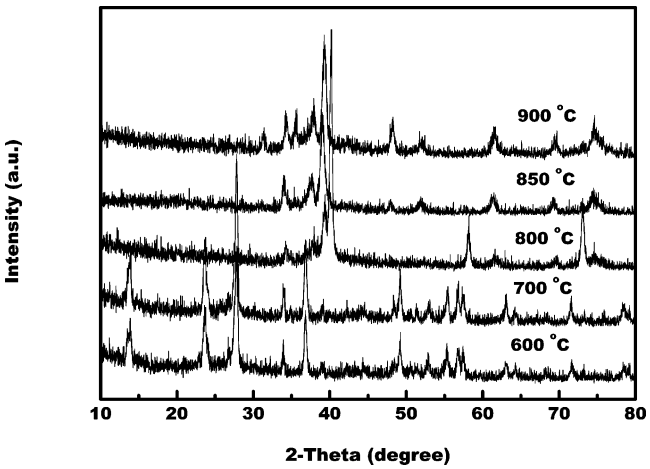

Figure 1. XRD patterns of WO_3/HSAC samples prepared by carbothermal reduction at different temperatures.

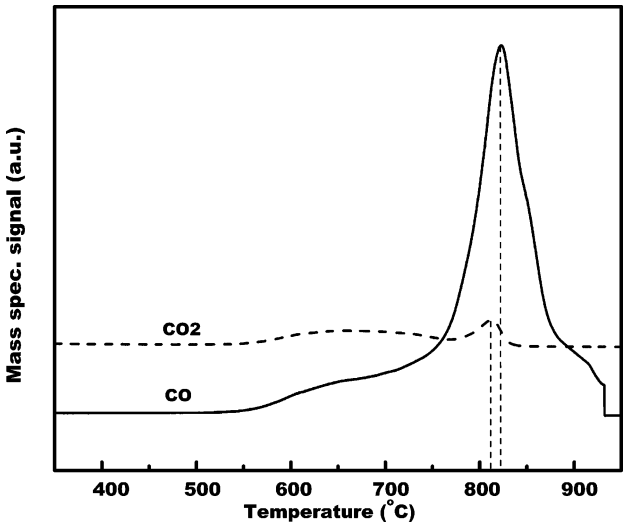

Figure 2. TPR−MS profiles of WO_3/HSAC sample in He flow.

Figure 2 shows the traces of masses 28 (CO) and 44 (CO_2) during carbothermal reduction of the WO_3/HSAC

sample. A broad and weak peak of CO_2 formation is in the range from 550 to 770 °C, and the corresponding CO signal is clear in this range. This indicates that WO_3 was progressively reduced to metal oxides with an oxidation state below (VI) or even metallic tungsten by carbon materials and/or the formed CO. With the increase of temperature, the peaks of CO and CO_2 reach the maximum intensity at about 820 and 810 °C, respectively. CO is mainly from WO_3 reduction reactions, which involves the following possible reactions:

$$WO_3 + C \rightarrow WO_2 + CO$$

$$WO_2 + C \rightarrow W + CO$$

while CO_2 is mainly from metal oxides reduction by CO and Boudouard reaction:

$$WO_3 + CO \rightarrow WO_2 + CO_2$$

$$WO_2 + CO \rightarrow W + CO_2$$

$$W + CO \rightarrow W_2C + CO_2$$

$$CO \rightarrow C^* + CO_2$$

(where C* is atomic carbon). Moreno-Castilla et al. found that the amount of CO evolved linearly increased with W content in WO_3 supported on activated carbon material, whereas the amount of CO_2 evolved is very low and independent of the W content, indicating the WO_3 particle was mainly reduced by carbon materials.[45] Therefore, it can be understood why the CO_2 signal is weak. It had been reported that the CO/CO_2 ratio influences the carburization reaction. In a CO_2-rich atmosphere, the carburization reaction stops at W_2C and reoxidation can even take place, whereas in a CO-rich atmosphere, the conversion to WC proceeds progressively through reaction between W_2C and atomic carbon (C*) or CO:

$$W_2C + C^* \rightarrow WC$$

$$W_2C + CO \rightarrow WC + CO_2$$

In these reaction conditions, the amount of CO is much more than that of CO_2 as determined from TPR−MS. Therefore, the carburization reaction does not stop at W_2C, and WC can be formed.

From XRD and TPR results, it can be concluded that WO_3 was reduced to metallic tungsten via $WO_{2.9}$ and WO_2, and metallic tungsten is further carburized to WC via W_2C. It is clear that the result is consistent with the assumed mechanism $WO_3 \rightarrow WO_{2.9} \rightarrow WO_2 \rightarrow W \rightarrow W_2C \rightarrow WC$ for the carbothermal reduction of WO_3 in the literature.[46] It is found that the mechanism of tungsten carbides from WO_3 and CH_4/H_2 also follows the above steps under the lower pressure reaction, whereas the WO_2 phase does not appear under the higher pressure.[47]

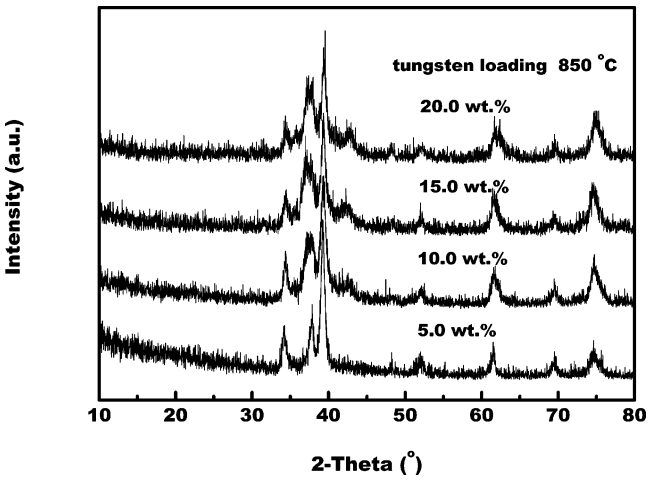

Figure 3. XRD patterns of WO_3/HSAC samples with different tungsten loadings prepared by carbothermal hydrogen reduction at 850 °C.

Synthesis of W_2C/HSAC via Carbothermal Hydrogen Reduction. Figure 3 shows XRD patterns of WO_3/HSAC samples with different tungsten loadings by carbothermal hydrogen reduction (CHR) at 850 °C. It is clear that the diffraction peaks at 34.32, 37.79, and 39.40° due to W_2C do not show clear change with increase of W loading. The average particle sizes of W_2C with 5, 10, 15, and 20 wt % W loading are 12, 12, 13, and 13 nm, respectively. The result is different from that obtained in Mo/HSAC, in which the particle sizes of β-Mo_2C increase with increasing Mo loading.[40] Moreno-Castilla et al. reported that the particle size of metallic tungsten-supported activated carbon is independent of the tungsten content.[48] This may be the main reason that the particle sizes of W_2C do not increase with increasing W loading.

Surface area, porosity, and average pore size of supported tungsten carbide samples are compiled in Table 1. It can be seen that the surface area, porosity, and average pore size of the samples decrease with increase of W loading. It can be assumed that tungsten precursor fills and blocks a fraction of the pores of carbon materials after carbothermal hydrogen reduction.

Figure 4 shows XRD patterns of WO_3/HSAC samples by carbothermal hydrogen reduction at different temperatures. XRD pattern of the sample with carbothermal hydrogen reduction at 500 °C does not show any diffraction peak, indicating that WO_x ($0 < x < 3$) is high dispersion. The well-dispersed WO_x may be due to the ultrahigh surface area and pore volume of the carbon material used in this study. The XRD pattern of the sample pepared by carbothermal hydrogen reduction at 600 °C shows a diffraction peak at 40.12° due to metal tungsten. In the case of the sample at 700 °C, diffraction peaks due to metal tungsten become sharper at 40.12, 58.29, and 73.18°. When the temperature increased up to 800 °C, the sharp peaks due to W_2C were detected at 34.32, 37.79, and 39.40°. Upon further increasing of temperatures of carbothermal hydrogen reduction to 850 °C, only diffraction peaks due to W_2C were observed. When the temperatures further increase, a mixed phase

(45) Alvarez-Merino, M. A.; Carrasco-Marin, F.; Fierro, J. L. G.; Moreno-Castilla, C. *J. Catal.* **2000**, *192*, 363.

(46) Gruner, W.; Stole, S.; Wetzig, K. *Inter. J. Ref. Metals Hard Mater.* **2000**, *18*, 137.

(47) Löfberg, A.; Frennet A.; Leclercq, G.; Leclercq, L.; Giraudon, J. M. *J. Catal.* **2000**, *189*, 170.

(48) Moreno-Castilla, C.; Alvarez-Merino, M. A.; Carrasco-Marin, F.; Fierro, J. L. G. *Langmuir* **2001**, *17*, 1752.

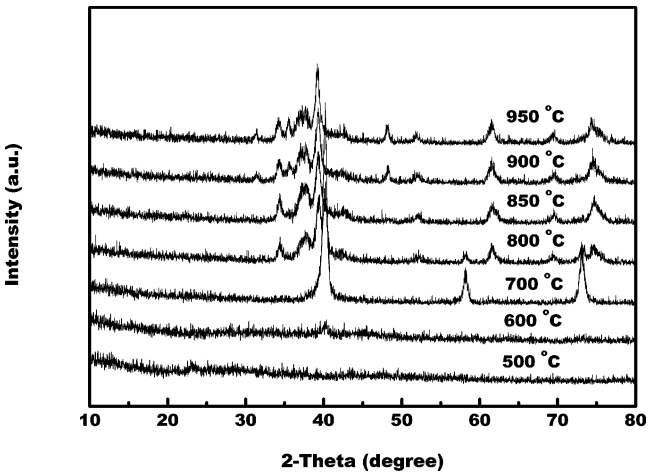

Figure 4. XRD patterns of WO_3/HSAC samples prepared by carbothermal hydrogen reduction at different temperatures.

of W_2C and WC can be obtained. The average particle sizes of metallic tungsten and W_2C may be estimated from the parameters of XRD according to the Scherrer formula. The average particle sizes of metallic tungsten at 700 °C and W_2C at 850 °C are about 14 and 12 nm, respectively. The typical TEM of the sample with carbothermal hydrogen reduction at 850 °C is shown in Figure 5a. It can be seen that the particle sizes of W_2C are about 10 nm in diameter dispersed on the outer surface of carbon materials, which is in agreement with the sizes obtained from XRD.

Figure 6 shows the profile of TPR−MS during carbothermal hydrogen reduction of WO_3/HSAC sample. The signals at M = 2 and 16 represent hydrogen and methane, and the signals at M = 18, 28, and 44 represent water, carbon monoxide, and carbon dioxide, respectively. The H_2 profile of the sample showed several broad peaks above 420 °C, indicating that there was a considerable amount of hydrogen consumption. The corresponding H_2O profile showed three peaks at about 550, 680, and 780 °C, with the peak at about 780 °C displaying the maximum intensity. H_2O evolution indicates that WO_3 was progressively reduced into metallic tungsten via oxides with low oxidation state.

$$WO_3 + H_2 \rightarrow WO_x + H_2O \ (3 > x > 2)$$

$$WO_x + H_2 \rightarrow WO_2 + H_2O$$

$$WO_2 + H_2 \rightarrow W + H_2O$$

But in the XRD result, no diffraction peak due to oxides with oxidation states below (VI) was detected and only peaks due to metallic tungsten were observed, indicating that the oxides with low oxidation state are well dispersed in ultrahigh-surface-area carbon materials. Löfberg et al. reported that the WO_2 phase does not appear when a CH_4/H_2 mixture was used as carburized reactant under the higher CH_4/H_2 pressure, which was attributed to rapid reaction ratio.[47]

The CO mass spectrometer signal appears when the temperature is above 450 °C, and shows two peaks at 800 and 810 °C. Meanwhile, a decrease in the hydrogen mass spectrometer signal accompanied by simultaneous water evolution was observed. CO formation is mainly due to carbothermal reaction between atomic carbon and W compounds in the presence of hydrogen.

$$WO_x + C^* + H_2 \rightarrow W_2C + CO + H_2O$$

In this reaction, W_2C was formed by the reaction between WO_x and CHy species from atomic carbon and hydrogen, which is similar to the process of Mo_2C formation.[40] In addition, CO can be also formed from carbon and water and CO_2 produced by reduction of the oxides.

$$C^* + H_2O \rightarrow CO + H_2$$

$$C^* + CO_2 \rightarrow 2CO$$

CO_2 and methane signals are broad and weak, and become clear above 750 °C. It can be assumed that CO_2 formation is from the following reaction in addition to the above reactions in carbothermal reduction.

$$CO/C^* + H_2O \rightarrow CO_2 + H_2$$

Methane evolution may be from hydrogenation of carbon and/or CO and CO_2.

$$C^* + 2H_2 \rightarrow CH_4$$

$$CO/CO_2 + 3H_2 \rightarrow CH_4 + H_2O$$

From the above TPR−MS result, it can be concluded that the introduction of H_2 into carbothermal reduction promotes the reduction of tungsten oxides and leads to tungsten carbides formation under relatively mild conditions.

Synthesis of W_2C/HSAC via Metal-Promoted Carbothermal Hydrogen Reduction. To synthesize tungsten carbides under much milder conditions, metal-promoted carbothermal hydrogen reduction (Ni−CHR) was studied. XRD patterns of WO_3/HSAC samples prepared by metal Ni-promoted carbothermal hydrogen reduction are shown in Figure 7. In those samples, the Ni/W molar ratio is about 0.2. It can be seen that no obvious diffraction peak was observed at 600 °C. It is obvious that the diffraction peaks due to W_2C can be detected even at 650 °C, which is about 150 °C lower than that in carbothermal hydrogen reduction in the absence of Ni. When the temperatures increase to 750 °C, the diffraction peaks become sharper, indicating that the particle sizes of W_2C increase with the increase of carbothermal hydrogen reduction temperature. The average particle size of W_2C at 750 °C is about 10 nm by metal Ni-promoted carbothermal hydrogen reduction, which is consistent with the result of TEM (Figure 5b). The samples only give diffraction peaks due to α-W_2C, and no diffraction peaks due to Ni were detected, suggesting Ni is in the framework of W_2C or highly dispersed in carbon materials. The diffraction peaks due to WC appear in the sample even at 850 °C. It is clear that addition of Ni further decreases formation temperatures of tungsten carbides (about 150 °C).

Figure 8 shows the TPR−MS profiles obtained with WO_3/HSAC samples prepared by metal Ni-promoted carbothermal hydrogen reduction. The H_2 profile of the

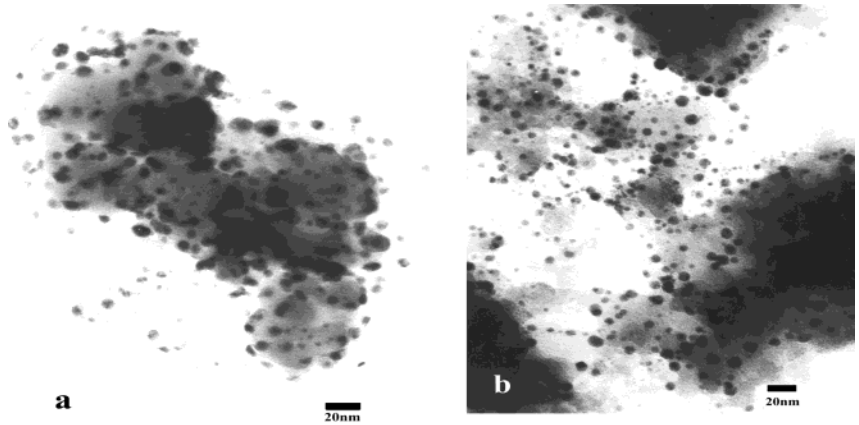

Figure 5. TEM micrographs of W_2C/HSAC samples prepared by carbothermal hydrogen reduction and metal Ni-promoted carbothermal hydrogen reduction.

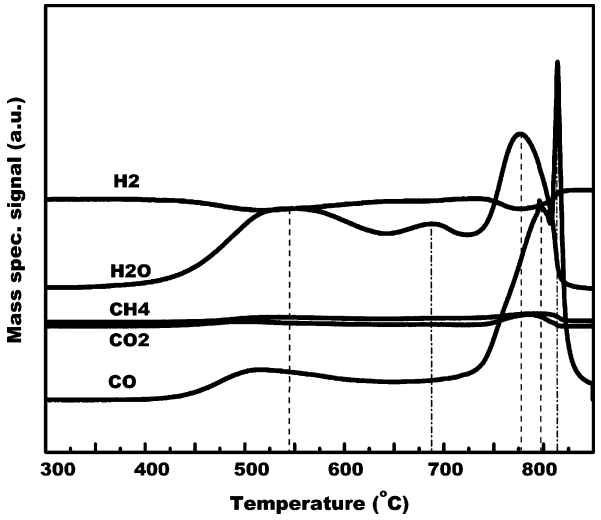

Figure 6. TPR−MS profiles of WO_3/HSAC sample prepared by carbothermal hydrogen reduction.

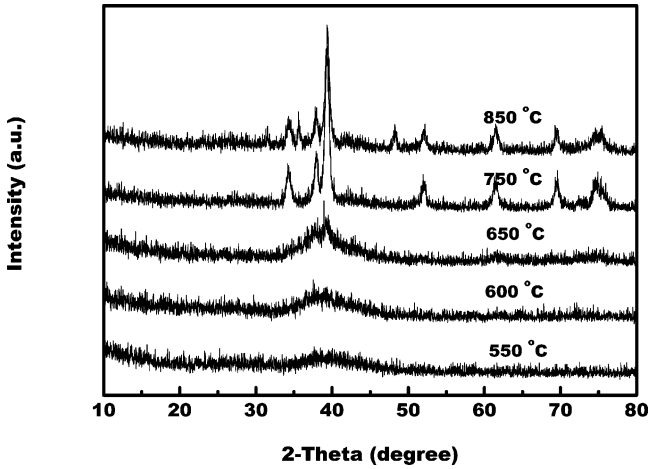

Figure 7. XRD patterns of WO_3/HSAC samples prepared by metal Ni-promoted carbothermal hydrogen reduction.

sample showed several broad peaks above 380 °C, indicating that there was a considerable amount of hydrogen consumption. The corresponding H_2O profile showed three peaks at about 450, 560, and 750 °C, which are lower than that in carbothermal hydrogen reduction. The result indicates that Ni promotes reduction of WO_3 at relatively low temperature. The CO mass spectrometer signal appears from 450 °C, further increases with the increasing temperature, and reaches the maximum at 770 °C. The temperature is lower than those in carbothermal hydrogen reduction, indicating that Ni also promotes CO formation from reaction between atomic carbon and W compounds in the presence of hydrogen.

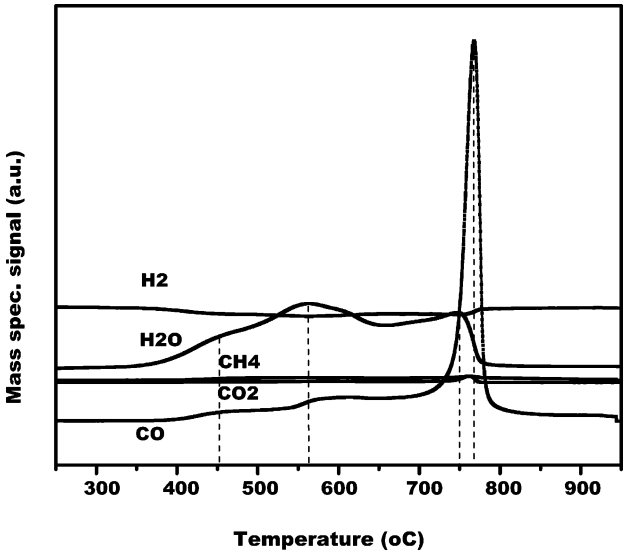

Figure 8. TPD−MS profiles obtained with WO_3/HSAC samples prepared by metal Ni-promoted carbothermal hydrogen reduction.

In addition, Co or Fe metal-promoted carbothermal hydrogen reduction also was used to synthesize nanostructured tungsten carbides. Similar effects were observed when Fe or Co metal was introduced into WO_3/HSAC samples. The addition of Fe or Co also decreases formation temperatures of tungsten carbides (about 150 °C). In the case of the sample with Co/W or Fe/W = 0.2, tungsten carbides can be detected by XRD when the temperature is above 650 °C. It is believed that metals, such as Ni, Fe, and Co, promote hydrogen disassociation and are favorable to formation of carbides.

Comparison among CR, CHR, and Ni−CHR for WCx/HSAC Synthesis. Table 2 shows comparisons of phase components and the molar fraction x of W_2C in a W_2C−WC−W mixture derived from CR, CHR, and Ni−CHR. It can be seen that pure W_2C phase can be formed at above 800 °C in CR and CHR, whereas pure W_2C phase can be formed even at 650 °C in Ni−CHR.

Table 2. Comparison of Phase Components and the Molar Fraction *x* of W_2C in a W_2C−WC−W Mixture Derived from Three Methods

temp. (°C)	CR	CHR	Ni−CHR
600	WO_3, WO_2, $WO_{2.9}$	W	no signal
650			α-W_2C
700	WO_3, WO_2, $WO_{2.9}$	W	
750			α-W_2C
800	W, α-W_2C (x = 0.18)	W, α-W_2C (x = 0.33)	
850	α-W_2C	α-W_2C	α-W_2C, WC (x = 0.89)
900	α-W_2C, WC (x = 0.83)	α-W_2C, WC (x = 0.82)	

Comparing the molar fraction x of W_2C in a W_2C−WC−W between CR and CHR, it is clear that W_2C formation is easier in CHR than in CR. Therefore, it can be concluded that WC_x formation is the easiest in Ni−CHR among the three methods.

The formation mechanism is similar although the three methods show the formation temperature is different. From XRD and TPR−MS results, it can be seen that WO_3 is first reduced into oxides with low oxidation states below (VI), and then further reduced into metallic tungsten. Metallic tungsten is carburized into W_2C through reaction with carbon materials and/or derivatives. Finally, WC can be formed through W_2C carburization. WO_3 reduction and metallic tungsten carburization are promoted in CHR and Ni−CHR, so that the temperature of WC_x formation is decreased by comparison with that of CR.

Adsorption of Thiophene on WC_x/HSAC. The removal of sulfur-containing compounds in gasoline and diesel has attracted attention because of very stringent environmental regulations. It is very difficult to reach ultra-deep desulfurization, although the conventional hydrodesulfurization (HDS) processes can remove the majority of sulfur-containing compounds.[49−51] To obtain ultralow-sulfur fuels, the conventional approaches will need to have increased catalyst bed volume at high-temperature and high-pressure conditions. The corresponding major problem is that the conventional HDS results in an increase of hydrogen consumption, high operation cost, and a significant decease of octane number, and so on. Therefore, some new desulfurization processes are being explored by research groups all over the world.[52−59] Adsorption is one of the most promising methods for ultra-deep desulfurization. Recently, the lay of surface alkylidenes can be formed by cycloketones adsorbed on a catalytically active surface of carbide and shows unprecedented thermal stability, indicating that it may be used as spacer groups for high-temperature applications, or chiral modifiers for asymmetrical heterogeneous catalysis.[19] In this work, we explored use of WC_x/HSAC as an adsorbent to remove sulfur-containing compounds in fuel oil. Figure 9 shows the sulfur concentration of the outlet as a function of adsorption time at room temperature on HSAC, W/HSAC, W_2C/HSAC, and WC/HSAC, respectively. In the case of HSAC, sulfur content reaches about 600 ng/mL after 30 min, indicating that HSAC has a very low capacity for thiophene adsorption. W/HSAC, W_2C/HSAC, and WC/HSAC samples show that no sulfur was detected after 30, 60, and 30 min, respectively, indicating that those samples have a high adsorption capacity for thiophene compared to HSAC, and the removal of sulfur can be attributed to adsorption of thiophene on W, W_2C, and WC. The adsorption of thiophene on tungsten carbides may be similar to adsorption of cyclobutanone on β-Mo_2C reported by McBreen et al.[19] It can also be seen that the adsorption capacity of W_2C/HSAC is the highest among the samples. The adsorption capacity of the samples on thiophene is in the following order: W_2C/HSAC > W/HSAC > WC/HSAC ≫ HSAC. The reasons for this order are not yet clear, but may be due to different particle size of carbides/metal and adsorption capability of tungsten carbides and metal. After thiophene adsorption reached saturation W_2C/HSAC was reduced for 2 h with H_2 at 800 °C. The W_2C/HSAC shows the same adsorption capacity for thiophene the second time. This result indicates that W_2C/HSAC as adsorbent of sulfur-containing compounds can be regenerated and reused. Therefore, nanostructured W_2C/HSAC may be of great potential in ultra-deep removal of sulfur-containing compounds in fuel oil.

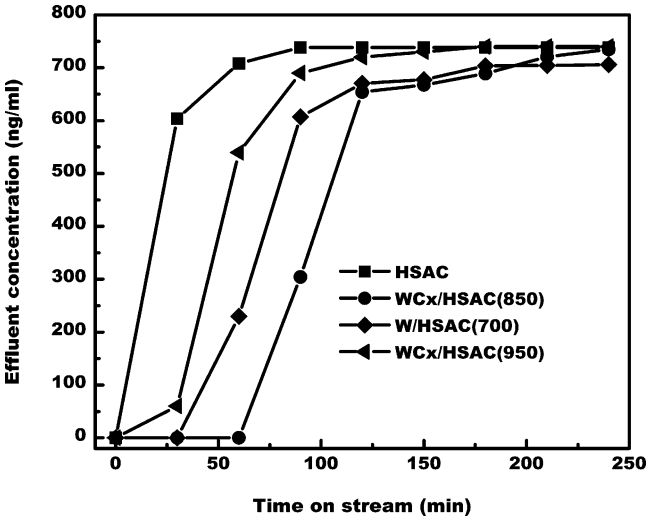

Figure 9. Sulfur concentration of the outlet as a function of adsorption time on HSAC, W/HSAC, W_2C/HSAC, and WC/HSAC.

(49) Whitehurst, D. D.; Isoda, T.; Mochida, I. *Adv. Catal.* **2000**, *42*, 345.
(50) Song, C.; Ma, X. L. *Appl. Catal. B* **2003**, *41*, 207.
(51) Babich, I. V.; Moulijn, J. A. *Fuel* **2003**, *82*, 607.
(52) Ma, X. L.; Sun, L.; Song, C. S. *Catal. Today* **2002**, *77*, 107.
(53) Shiraishi, Y.; Naito, T.; Hirai, T.; Komasawa, I. *Chem. Commun.* **2001**, *14*, 1256.
(54) Shiraishi, Y.; Taki, Y.; Hirai, T.; Komasawa, I. *Ind. Eng. Chem. Res.* **2001**, *40*, 1213.
(55) Yang, R. T.; Takahashi, A.; Yang, F. H. *Ind. Eng. Chem. Res.* **2001**, *40*, 6236.
(56) Yazu, K.; Yamamoto, Y.; Furuya, T.; Miki, K.; Ukegawa, K. *Energy Fuels* **2001**, *15*, 1535.
(57) Milenkovic, A.; Schulz, E.; Meille, V.; Loffreda, D.; Forissier, M.; Vrinat, M.; Sautet, P.; Lemaire, M. *Energy Fuels* **1999**, *13*, 881.
(58) Bosmann, A.; Datsevich, L.; Jess, A.; Lauter, A.; Schmitz, C.; Wasserscheid, P. *Chem. Commun.* **2001**, *23*, 2494.
(59) Aitani, A. M.; Ali, M. F.; Al-Ali, H. H. *Petrol. Sci. Technol.* **2000**, *18*, 537.

Conclusions

Nanostructured W_2C with particle size of about 10 nm on high-surface-area carbon material has been synthesized by carbothermal reduction and carbothermal hydrogen reduction at 850 °C, and addition of hydrogen into the carbothermal reduction promotes reduction of tungsten oxides and formation of tungsten carbides. Nanostructured W_2C has also been obtained by metal Ni-promoted carbothermal hydrogen reduction even at 650 °C, and addition of Ni decreases formation temperatures of tungsten carbides. The formation of tungsten carbides includes the following steps: reduction of WO_3 into oxides with low oxidation states below (VI), reduction of the oxides into metallic tungsten, carburization of metallic tungsten into W_2C, and carburization of W_2C into WC. W/HSAC, W_2C/HSAC, and WC/HSAC samples show high capacity for thiophene adsorption compared to HSAC, and the removal of sulfur can be attributed to adsorption of thiophene on W, W_2C, and WC. Nanostructured W_2C/HSAC may be of great potential in ultradeep removal of sulfur-containing compounds in fuel oil.

Acknowledgment. We are grateful to the Ministry of Science and Technology of the People's Republic of China (State Key Project for Basic Research & Development with Grant G2000048003) for financial support.

CM034399C